

Batteries to Keep Solar-Driven Water Splitting Running at Night: Performance of a Directly Coupled System

Li-Chung Kin, Oleksandr Astakhov, Minoh Lee, Stefan Haas, Kaining Ding, Tsvetelina Merdzhanova,* and Uwe Rau

Direct solar-powered hydrogen generation (so-called “green” hydrogen) is promising as a renewable fuel that can be generated anywhere there is sunshine and water. Many attempts are made to integrate a water electrolyzer (EC) and solar cell at different levels (a so-called artificial leaf) to take advantage of the reduced losses from the lack of wiring and optionally increased portability afforded by an integrated unit. However, in many cases, EC catalysts degrade as electrodes depolarize when shut down at night. Much less attention is paid to the need for a minimum current across the EC under insufficient illumination to prevent excessive cyclic degradation. Directly coupling a battery to keep an artificial leaf running at night can address this need and, in theory, also increase solar-to-hydrogen (STH) efficiency. A seven-cell silicon heterojunction module, two bifunctional NiFeMo ECs in series, and a commercial Li-ion NMC battery are selected to provide the same amount of solar output power despite different working voltages and tested in a series of simulated diurnal cycles. The increased average STH efficiency per cycle (11.4% vs. 10.5% without the battery) is analyzed and discussed with implications for future artificial leaf design and implementation.

1. Introduction

Solar-driven water electrolysis has been considered a promising way of converting light energy to chemical energy, in the form of hydrogen gas, that can be used in different ways upon demand.^[1,2] Among different types of solar water-splitting

approaches,^[3–6] the photovoltaic–electrochemical (PV–EC) system, or artificial leaf, has shown the highest solar-to-hydrogen (STH) efficiency of over 30%^[7] and has been considered the most appropriate way for commercialization in the near future.^[2] Water-splitting performance of the PV–EC device is determined by the intersection of the polarization curve of the electrolyzer and the I – V characteristic of the PV cell or module,^[8,9] which sets the working point of the artificial leaf.^[8,10]

It is widely accepted that a lower operating current density of the electrolyzer, either by lowering the working voltage or by vastly increasing the active surface area, will not only increase longevity of the system but also increase the efficiency.^[11–13] However, lowering the working voltage results in a corresponding decrease in hydrogen produced and increasing the area


of the catalyst often requires complex coating procedures^[14] or an uneconomical increase in the loading of the catalyst. Most artificial leaf^[15] solar electrolyzers are designed to work on the premise that the system only generates hydrogen during illumination and most of them are optimized for a specific irradiance. However, natural diurnal irradiance variation, sudden drops of irradiance related to the state of the atmosphere, and, cloudiness can cause rapid fluctuations of the electrolyzer current that results in electrode depolarization.^[16] Previous research has shown that the electrolyzer performance and durability can be adversely affected by on–off cycles^[16] and a small protective current is recommended to prevent increased catalyst dissolution due to electrode depolarization caused by voltage cycling.^[17]

One straightforward measure to stabilize operating conditions of the electrolyzer is to include battery storage into the PV–EC combination, turning it into the PV–EC–Battery (PEB) system, as demonstrated at the residential system level.^[18] In our previous work,^[19] we have explored how storage can be included in a directly connected PV–EC system. We have shown the feasibility of unaided operation of a cell-to-cell, directly connected PEB system. It has been shown theoretically and experimentally that a battery connected in parallel to the EC cell can smoothen out the PV power fluctuations, facilitate power coupling, and even improve STH efficiency. The latter point shown theoretically^[19] is of particular interest but is yet to be shown experimentally. Analysis of the PEB system operation shows that the distribution

L.-C. Kin, O. Astakhov, S. Haas, K. Ding, T. Merdzhanova, U. Rau
Institut für Energie- und Klimaforschung (IEK-5)
Forschungszentrum Jülich GmbH
52428 Jülich, Germany
E-mail: t.merdzhanova@fz-juelich.de

M. Lee
Department of Mechanical and Industrial Engineering
University of Toronto
Toronto, Ontario M5S 3G8, Canada

U. Rau
Faculty of Electrical Engineering and Information Technology
RWTH Aachen University
Mies-van-der-Rohe-Straße 15, 52074 Aachen, Germany

 The ORCID identification number(s) for the author(s) of this article can be found under <https://doi.org/10.1002/solr.202100916>.

© 2022 The Authors. Solar RRL published by Wiley-VCH GmbH. This is an open access article under the terms of the Creative Commons Attribution License, which permits use, distribution and reproduction in any medium, provided the original work is properly cited.

DOI: 10.1002/solr.202100916

of the PV-generated energy over the whole diurnal cycle of operation results in a noticeable reduction of the power delivered to the electrolyzer for the same amount of solar energy collected. This facilitates reduction of the overpotential loss in the electrolyzer and consequently increases the overall STH efficiency despite the voltage loss inevitably associated with the battery charge–discharge cycle.

In this work, we present an experimental proof of concept of our previously described theoretical framework^[19] by coupling a solar electrolyzer with a working voltage matched to that of an appropriately sized battery. We compared two situations using exactly the same solar electrolyzer setup, under the same duration of illumination, with and without a battery attached. By working on both sides of the solar module maximum power point (MPP), we also exclude effects associated with different output power to the two systems working at different voltages by ensuring that the coupling factors of both systems' working points are almost identical. Combining a shingled seven-cell silicon heterojunction solar module with a pair of Earth-abundant NiFeMo catalyst^[20] electrolyzers in series and, a commercial Li-ion battery, we show that such a system not only works as expected but can be done with relatively inexpensive, accessible, and abundant materials.

2. The Concept

As detailed by Astakhov et al.,^[19] if the current from solar illumination can be stored and used later during the night, a solar electrolyzer should see efficiency gains from working at a lower voltage working point. In **Figure 1**, a battery attached to an artificial leaf will store part of the charge collected in the day (Q_B), to be released to the electrolyzer at night for conversion into hydrogen (Q_{H2d}) at a lower current rate ($I_{ECd} < I_{BI}$), but over a longer time. By coupling a solar electrolyzer^[20] in parallel to a battery (PEB) of sufficient size and voltage, the total current density in the electrolyzer can be reduced during illumination but a higher current is drawn from the PV module. Running the electrolyzer on the battery-stored energy in the night, all charge collected during illumination (Q_B) can be utilized to split water if the battery has no charge losses, and the discharge

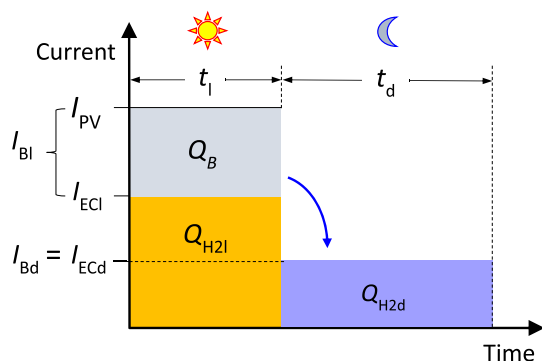


Figure 1. Charge conservation and relative current levels within the PEB test. Ideally charge is conserved by the battery (Area Q_B = Area Q_{H2d}) during the “day” (t_l) and released over a longer time at “night” (t_d) for one diurnal cycle.

current, I_{Bd} , is sufficiently high to release all the charge before the next cycle.^[19]

The first condition is achieved by very high Faradaic (Coulombic) efficiencies in modern batteries exceeding 99% per cycle.^[21,22] This is especially so for low state of charge utilization and relatively low C-rates (battery charge/discharge rates relative to 1 h for full charge) for charge and discharge below 1 C. The second condition is fulfilled when the product $I_{Bd} \times t_d$ equals or exceeds Q_B after accounting for storage and transmission losses. In the experiment, we control the discharge time to achieve exact charge balance to assess the change in STH efficiency accurately.

In **Figure 2a**, without the battery, the solar module (PV) only powers the electrolyzer (EC) under illumination (P_{ECI}) to generate hydrogen (P_{H2l}). With the battery attached, power diverted from the PV to the battery under illumination (P_B) will be used to power the electrolyzer (EC) in the dark (P_{ECd}) and result in two-time-resolved streams of hydrogen for the light (P_{H2l}) and

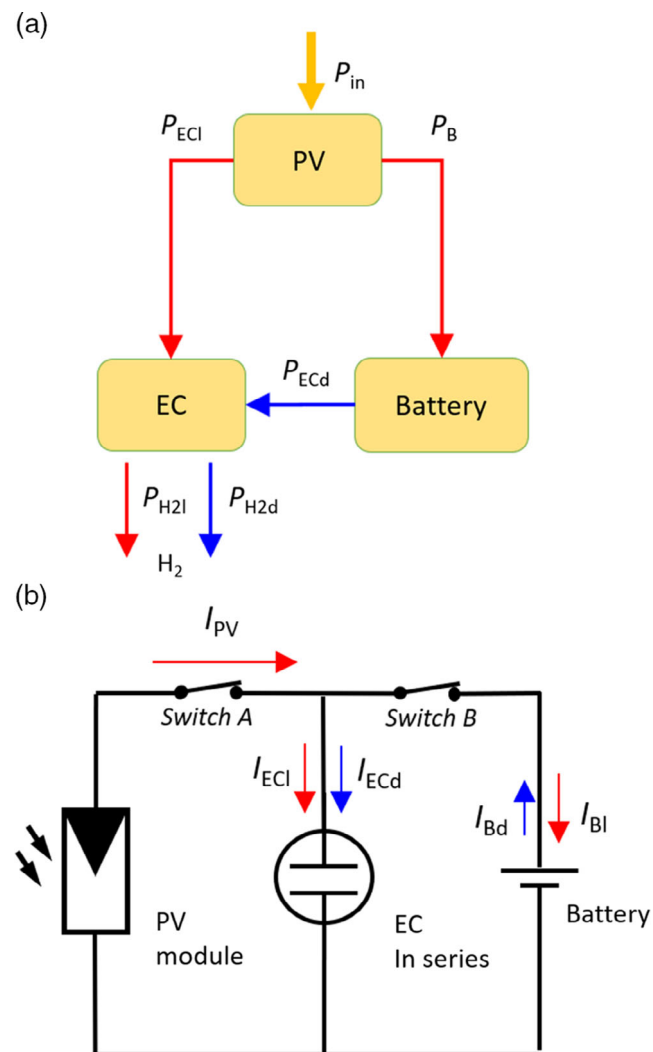


Figure 2. a) Power flow and b) circuit diagram for the experimental system. For the PV–EC test, switch B will be open to exclude the battery. For the PEB test, both switches will be closed under illumination, and switch A will be open during the dark period.

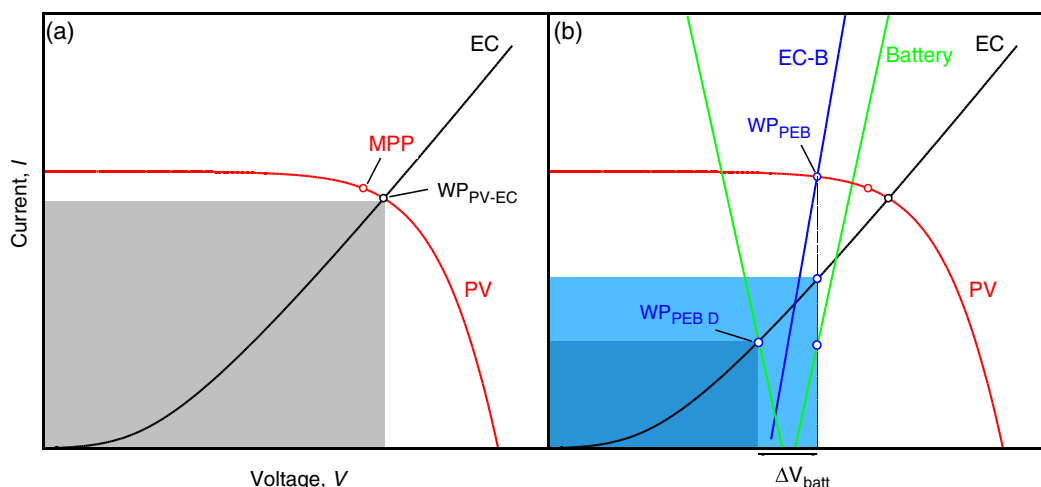


Figure 3. Illustrative curves for a photovoltaic module directly paired with a) an electrolyzer (PV–EC) and b) with a battery attached in parallel (PEB).

dark (P_{H2d}) times of operation. This is achieved experimentally with all three components connected in parallel, (Figure 2b) each having their own respective voltmeters and ammeters (not shown). Using switches, A and B, we can switch between PV–EC and PEB tests with and without illumination. With both switches closed under operating conditions with the battery attached (PEB) and switch B open for operation without the battery (PV–EC) as a comparison, to simulate dark conditions with the battery attached, switch A is opened and the light is turned off after the illumination step (PEB dark) and the battery discharges across the electrolyzers.

The experimental setup detailed earlier enables us to realize the dual modes of operation using a single setup without stopping the experiment to switch between PV–EC and PEB modes of operation. This enables both respective current–voltage profiles detailed in **Figure 3a,b** to be realized with one setup. In **Figure 3a**, showing a PV–EC system, a hypothetical example EC (black curve) and PV module (red curve) together will result in a working point at the intersection of the two curves (WP_{PV-EC}) under illumination. With the onset voltage of hydrogen evolution set at the left vertical axis, the area encompassed by the gray square at the working point represents the total voltage-related kinetic loss for hydrogen generated at this working point.

Adding an appropriate hypothetical battery (**Figure 3b**, light green curve) to transform the PV–EC system in **Figure 3a** to a PEB system should shift the working point of the PV–EC system under illumination to a lower-voltage working point determined by where the new load curve (blue curve, EC-B) intersects the PV curve (WP_{PEB}). The PV current at this lower voltage is always higher than before due to the shape of the PV curve, even if it was working at the PV MPP before. The current, however, is now split between the battery and the EC. The current going into the EC is determined by the vertical intersection of the new working point and the initial EC curve with the battery charging current, making up the difference between these two points. This results in lower kinetic losses illustrated by the blue overlapping shaded regions, which sum up to a smaller area than before. Essentially, adding a battery is equivalent to working above the EC curve without adding more catalyst or increasing catalyst

loading with the condition that all the current stored is utilized in the water-splitting reaction later.

In the directly coupled PEB device presented in **Figure 3b**, the voltage efficiency loss from the battery charge–discharge overpotential (ΔV_{batt}) is directly offset by the voltage efficiency gain from the electrolyzer. The lower PEB working voltage for the same amount of energy/power input results in an increase in total current, and thus total charge converted to hydrogen, leading to a net gain in hydrogen produced.

The working point during illumination shifts from the black point before attachment (WP_{PV-EC}) to the blue point after attachment of the battery (WP_{PEB}). Working currents with the battery attached are found from the vertical intersection of WP_{PEB} and the EC curve and battery charge curve. In the dark, the working point for the electrolyzer shifts to the intersection between the battery discharge curve ($WP_{PEB D}$). Letting the left axis be E^0 , where E^0 is the reversible cell voltage of water splitting at standard conditions (in our case, $E^0 = 2 \times 1.23V$ for a pair of electrolyzers in series), the shaded boxes indicate the kinetic losses associated with each scenario, while the battery charge–discharge overpotential is shown by ΔV_{batt} . Note that the areas of both rectangles in plot b) are generally not indicative for the energy analysis because they represent powers acting for different periods of time.

3. Results and Discussion

The PV component of the system is represented by a seven-cell silicon heterojunction module (SHJ) minimodule with an open-circuit voltage of 5.05 V, short-circuit current of 114.9 mA, and 19.9% efficiency. The MPP is located at MPP voltage of 4.1 V and MPP current of 108 mA. Current–voltage characteristics of the PV module are presented by the blue curve (**Figure 4**). The EC polarization curve is plotted in gray and mirrored about the x-axis for clarity with the red line (EC dark) representing the same curve operating on battery power in the dark.

Connecting only the EC during illumination (PV–EC mode), an average current of 96 mA was measured, passing through the EC at 4.23 V (gray square, PV–EC_{EC}), while the PV working

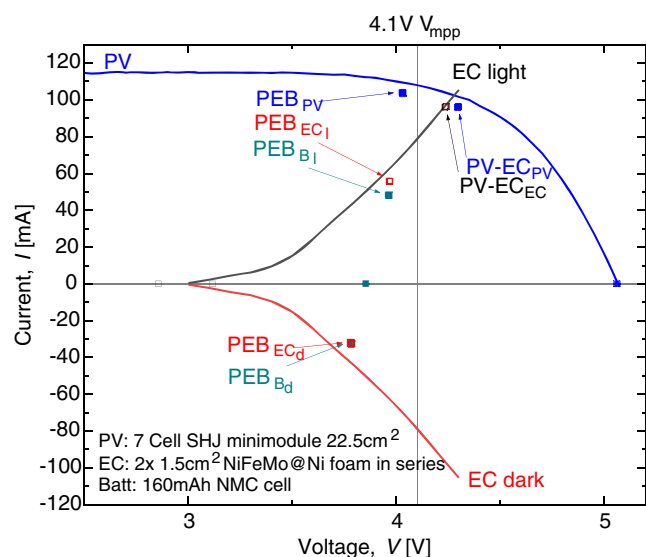


Figure 4. Current–voltage curves for the seven-cell PV module and the two EC cells in series; each electrolyzer has an electrode area of 1.5 cm². The different working points can be seen for both the PV–EC and PEB modes. The dark operation (subscript d) mode of the PEB setup is depicted as having negative current for clarity.

point was 96 mA at 4.29 V (blue square, PV–EC_{PV}). The PV working points (blue squares) are not on the curve as these are all measured in the two-wire mode, whereas the curve is measured in the four-wire mode, excluding series resistance. Upon connecting the battery (PEB mode), the PV working point was seen to shift to 4.03 V and 103.5 mA (PEB_{PV}), while the EC working point was 3.96 V and 56.2 mA (red square, PEB_{ECI}) and the battery charged at 3.96 V and 47.3 mA (teal square, PEB_{BI}). For the PEB measurement, this agrees with the concept where the total current is split between PV and EC during illumination and the operating voltage is pinned to the lower battery charging voltage.

The PV–EC test ran at a higher voltage than that of the PEB test, but the total current from the PEB test is higher. The effective working point of the PEB system exceeds the possible electrolyzer (EC) current–voltage curve during illumination, with the total current split between the battery and the EC in an ≈45:55 ratio.

In the dark, for the PEB mode, the battery discharges through the EC, resulting in the working points of the battery (PEB_{Bd}) and electrolyzer (PEB_{ECd}) overlapping. The EC operates at a significantly lower voltage when powered by the battery due to the battery's inherent overpotential loss. Although there is a loss in energy from voltage overpotential loss from the battery, this is exactly compensated by the reduced overpotential loss in the EC cell, and total overpotential losses during light and dark periods are the same in the PEB system, as we described in detail in our previous work.^[19] This can be understood simply by considering the initial PV input potential during illumination, and the final hydrogen generation potentials are unchanged and are both independent of the intermediate storage potential.

Using the same solar module and the same electrolyzer under the same conditions with and without a battery attached is meaningless without considering the working point and the

corresponding PV coupling factor. Different working voltages will cause the PV power output to change. Coupling factor can be thought of as the proportion of maximum power output of the PV element that is utilized at a constant working voltage and will determine the total input power into the EC and/or battery during one diurnal cycle. Coupling factor is related to the use of the total proportion of the maximum power of the PV input. Beyond the direct effect on total input power supplied to the electrolyzer and/or battery in the particular illuminated period, coupling has no direct effect on the operation of the EC cell in the night, while being under battery power. Coupling factor can be omitted at night, as the PV input is zero. Thus, it is important to keep a constant coupling factor, C , between both tests defined by the following relation.

$$C = \frac{P_{pv}}{P_{mpp}} \quad (1)$$

where P_{pv} is the power output at the working point of the PV module and P_{mpp} is the MPP power output. Any value below 1 means that the power generation potential of the PV device is not fully utilized.

To determine the impact on the addition of the battery to the STH efficiency, the amount of energy delivered by the PV module should be the same in both scenarios. This is done by ensuring that the illumination time and the coupling factor of both modes are as close to identical as experimentally possible.

In **Figure 5**, we can see that the coupling factors, C , of the PV–EC test and the PEB tests were almost identical at 0.925 and 0.932 on average. This results in a PV power output that is almost constant across both tests during illumination despite the PV–EC working at 4.4 V and the PEB working at ≈4 V. The splitting of current between battery and solar cell also results

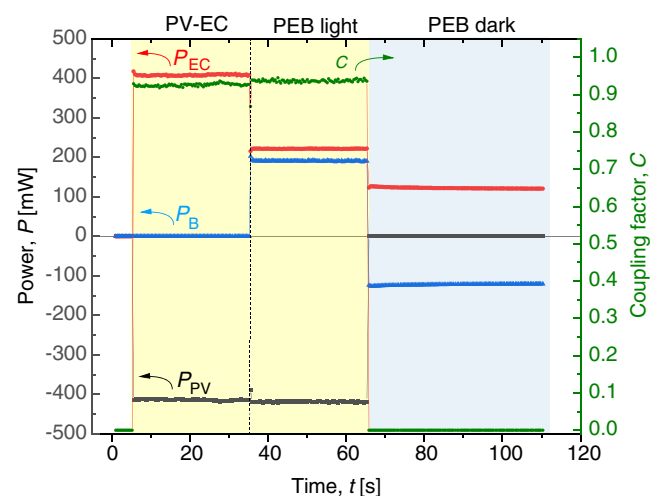


Figure 5. Representative power and coupling factor versus time curves for both experiments show almost identical PV power output and coupling factor for both PV–EC and PEB tests. Each cycle is run by first having a reference measurement of PV–EC for a set time (30 s) and then immediately connecting the battery and beginning the PEB experiment for the same amount of illuminated time. Discharge time is automatically determined by software charge counting and three cycles were run this way, assuming 100% Coulombic/Faradaic efficiency of the battery.

in less-noisy power output at the EC cell likely due to lower bubble-related loss,^[23] due to a lower current density across the EC cell in both the light and dark parts of the test. Software charge counting was used to automatically determine the time required to discharge the battery back to its original state of charge to complete a single diurnal cycle with 100% charge utilization. Note that the variation of power for the PV–EC system is from 0 to 400 mW, while the power fluctuates between 100 and 220 mW for the PEB system.

3.1. Comparing PV–EC and PEB Systems' Energy Output

By plotting the energy input and output from the electrolyzer of both systems to the voltage, the difference of the two tests' run time can be effectively reconciled. In **Figure 6**, we plot the solar energy input as E_{PV} and hydrogen energy output from the electrolyzer as $E_{H_2\text{ PV}}$. These represent the boundaries of maximum energy input and output of the system in one diurnal cycle.

Here we can see clearly that the voltage of the PEB system is always lower than that of the PV–EC system, thus having a higher electrolyzer voltage efficiency^[24–26] throughout 58.1% compared with 62–65.1% (voltage efficiency = $E^0/V_{EC} \times 100\%$). Furthermore, we can see that the voltage drop of the battery from charge to discharge is inconsequential as the electrolyzer runs for a longer time at a lower potential.

Figure 6 also shows that the total amount of energy input into the electrolyzer for both cases is almost identical with a difference of 0.6%. The PEB has a slightly lower energy value ($E_{PEB} < E_{PV-EC}$) due to the addition of the battery and additional wiring adding some losses to the system. However, looking at the

amount of H_2 produced, there is a total increase in 8.4% ($E_{H_2\text{ PEB}} > E_{H_2\text{ PV-EC}}$). Due to the lowered working PV voltage for the PEB system, which is more or less pinned to the charging voltage of the battery, the nearly identical energy supplied by the PV module results in a higher amount of charge delivered to the electrolyzer. Furthermore, the lower current density across the electrolyzer electrodes leads to more efficient hydrogen production. Attaching a battery is thus akin to having a larger- or higher-efficiency electrolyzer. In the PEB tests, 53.8% of hydrogen was produced under illumination and 46.2% was produced under battery power.

As the x-axis in Figure 6 starts at E^0 , the voltage between the y-axis and the two vertical lines in the PEB curve represents the overpotential losses of the EC for each mode of operation. As the battery and electrolyzer are in parallel, the operating voltages also reflect the charge–discharge voltage of the battery and thus the difference between them also represents the battery overpotential loss. Note that the electrolyzer overpotential in the dark is lower than under illumination by the battery overpotential loss.

3.2. STH Efficiency

STH conversion efficiency (η_{STH}) is commonly used to quantify the performance of solar electrolyzers under standard conditions of AM1.5G irradiance (100 mW cm^{-2}) and no applied bias.^[27] It is commonly defined as the ratio of the amount of chemical energy produced and the amount of solar energy incident on the solar cell/module.

$$\begin{aligned}\eta_{STH}(\%) &= \left[\frac{\text{Chemical energy output}}{\text{Solar energy input}} \right] \\ &= \left[\frac{\text{Rate of } H_2 \text{ production } \Delta G_{H_2O \rightarrow H_2 + \frac{1}{2}O_2}}{P_{in} \cdot A_{PV}} \right] \\ &= \left[\frac{I_{PV} \times E^0 \times \eta_F}{100\text{ mW cm}^{-2} \times A_{PV}} \right]_{AM1.5G}\end{aligned}\quad (2)$$

where η_F is the Faradaic efficiency of the electrolyzer, E^0 is the reversible cell voltage of water splitting at standard conditions, I_{PV} is the current of the solar cell/module and of area A_{PV} , under incident solar power density P_{in} . This can also be seen simply as a product of the efficiencies of both the electrolyzer and the PV module and PV coupling factor.

$$\eta_{STH}(\%) = \eta_{EC}(\eta_{PV}C) \quad (3)$$

However, these two equations are not directly applicable to the PEB system as the total time the EC is run and the total time under illumination has been decoupled. Also, as the tests are run back to back with no break, it was also not possible to accurately split the streams of gas for direct comparison; thus, an assumption of perfect Faradaic efficiency of the catalyst ($\eta_F = 100\%$) is used to simplify the analysis. This assumption helps to isolate gains and losses to the change in the system from specifically adding the battery. Nonideal catalyst Faradaic efficiency, as long as it is more or less constant between the two working modes, will not meaningfully affect the analysis, as they can be considered constant factors. Instead, comparing total chemical energy evolved and light energy

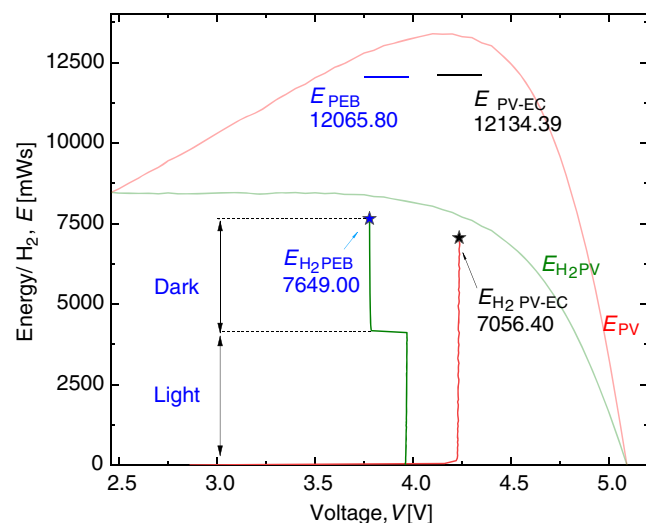


Figure 6. Solar energy input and solar-generated hydrogen curves plotted against voltage for one representative diurnal cycle. Overall solar energy collected by the PEB system is lower than the PV–EC system but results in more H_2 produced. Lines plotted below the final amounts of energy collected (stars) trace out the energy collected over time to distinguish the energy produced during the dark (E_{H_2d}) and light (E_{H_2l}) working stages of the PEB test and their respective working voltages. Note that the x-axis begins from double the thermodynamic potential of water splitting at standard conditions (E^0).

captured in both PV–EC and PEB is more instructive.

$$\eta_{\text{STH PV-EC}}(\%) = \left[\frac{E_{\text{H}_2 \text{ light}}}{E_{\text{total}}} \right] = \left[\frac{\int_0^t I_{\text{EC light}} dt \cdot E^0 \cdot \eta_F}{P_{\text{in}} \cdot A_{\text{PV}} \cdot t_1} \right]_{\text{PV-EC}} \quad (4)$$

$$\eta_{\text{STH PEB}}(\%) = \left[\frac{E_{\text{H}_2 \text{ light}} + E_{\text{H}_2 \text{ dark}}}{E_{\text{total}}} \right] = \left[\frac{(\int_0^t I_{\text{EC light}} dt \cdot E^0 \cdot \eta_F) + (\int_{t_1}^t I_{\text{EC dark}} dt \cdot E^0 \cdot \eta_F)}{P_{\text{in}} \cdot A_{\text{PV}} \cdot t_1} \right]_{\text{PEB}} \quad (5)$$

where $E_{\text{H}_2 \text{ light}}$ and $E_{\text{H}_2 \text{ dark}}$ refer to the amount of hydrogen energy produced. E_{total} is the total energy incident on the solar module of area A_{PV} , with incident solar power density P_{in} for the test duration under AM 1.5G illumination solar irradiation. Total illumination time of the respective systems is t_1 and total experimental time is t .

Under certain circumstances, simplified analysis gives acceptable results which can be used for a quick check of the system at the design stage to save time and effort. For the analysis of rectangular irradiance profiles, battery Coulombic/Faradaic efficiency of 100% are assumed. Equation (5) also can be simplified for the case of the rectangular irradiance profile to a simple sum of currents to the electrolyzer and battery during the illumination phase.^[19]

$$\eta_{\text{STH PEB}}^*(\%) = \frac{E^0 \cdot I_{\text{ECBI}}}{P_{\text{in}} \cdot A_{\text{PV}}} \quad (6)$$

where $I_{\text{B light}}$ is the current into the battery during illumination and I_{ECBI} is the total current input to the battery and electrolyzer under illumination (or in lossless circuits, the PV current, I_{PV} may be used).

From Equation (4) and (5), we obtain the STH efficiencies of both systems, showing an absolute increase of 0.88% with the addition of the battery.

$$\eta_{\text{STH PV-EC}}(\%) = \left[\frac{E_{\text{H}_2 \text{ PV-EC light}}}{E_{\text{total}}} \right] \quad (7)$$

$$= \frac{7056.40 \text{ mWs}}{100 \text{ mW cm}^{-2} \times 22.4 \text{ cm}^2 \times 30 \text{ s}} = 10.50\%$$

$$\eta_{\text{STH PEB}}(\%) = \left[\frac{(E_{\text{H}_2 \text{ PEB light}} + E_{\text{H}_2 \text{ PEB dark}})}{E_{\text{total}}} \right] = \frac{7649 \text{ mWs}}{100 \text{ mW cm}^{-2} \times 22.4 \text{ cm}^2 \times 30 \text{ s}} = 11.38\% \quad (8)$$

Comparing these values to Equation (6)

$$\eta_{\text{STH PEB}}^*(\%) = \frac{(2 \times 1.23 \text{ V}) \times 104.13 \text{ mA}}{100 \text{ mW cm}^{-2} \times 22.4 \text{ cm}^2} = 11.44\% \quad (9)$$

We can see that $\eta_{\text{STH PEB}}^*(\%)$ and $\eta_{\text{STH PEB}}(\%)$ differ by only 0.06%, and thus this proves that the method proposed in our earlier work^[19] is sound and the simplified lossless analysis can be used as a good approximation of the total efficiency of a PEB system for the fast optimization or comparison of different PEB systems. Equation (6) is much more convenient as instantaneous

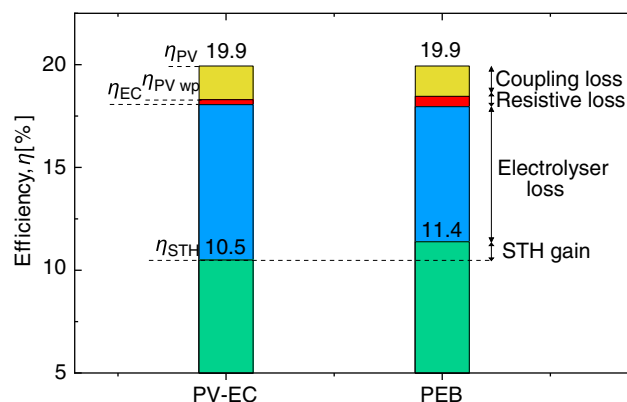


Figure 7. Energy loss analysis of the two systems showing the various cumulative losses from the solar module efficiency, leading to the final STH efficiency.

current and power values during illumination can be used without running the whole system for a full diurnal cycle or can even be estimated at the design phase from the PV curve without running the experiment.

3.3. Energy and Loss Analysis

By plotting the maximum efficiencies at each device following the schematic in Figure 6, we can estimate the losses associated with each stage of energy conversion. In Figure 7, this is reflected in the maximum values at the top of each colored bar, with values obtained without the battery on the left (PV–EC) and with the battery attached on the right (PEB). There is a significant but almost equal loss in energy efficiency from utilizing the PV module away from its MPP (19.9%) to their respective working points of 18.3% and 18.5% as per experimental design, represented by the coupling loss. Next is the red portion, which is the delta in efficiency from the PV output and EC input voltage and currents. This is generalized as being resistive losses. Because the power through the batteries is also an electrolyzer input, any losses from the batteries manifest as a larger “resistive loss.”

Note that in this analysis Faradaic/Coulombic losses from the battery are excluded due to charge counting, and voltage losses from the battery are compensated directly by the electrolyzer upon production of hydrogen. The low losses from battery storage are rather expected, given that the size of the battery (160 mAh) and total utilization of the battery during charge was ≈ 0.392 mAh or less than 1% maximum capacity at a charge rate of 47 mA (0.294 C-rate) and discharge rate of 33 mA (0.2 C-rate).

The blue portion of the graph details the power entering the electrolyzer, while the green portion is the final STH efficiency of both systems, with the ratio between them giving the efficiency of the electrolyzer and the loss given by the delta between the two thresholds. Note that in this analysis the total efficiency of the PEB is an average of the voltage efficiency of the light and dark times. From here it is clear that the addition of the battery causes η_{STH} to increase via the increased efficiency of the electrolyzer. Using the battery to store charge, the positive relationship between voltage and efficiency of an electrolyzer is effectively decoupled.

4. Conclusion

In our work, a battery has been added in parallel to an artificial leaf (PV–EC system) without power electronics for continued operation in the dark. The main function of the battery is to ensure electrolyzer current throughout the diurnal operation cycle to prevent depolarization of the electrolyzer when illumination is insufficient. In a broad sense, it is also a logical extension of the PV–EC system to realize a sustainable combination of PV generation with short- and long-term storage.

We demonstrate that a simple parallel connection of a battery system is sufficient for the self-sustained operation of the artificial leaf without power conversion or matching electronics. The battery voltage effectively sets the working voltage of the artificial leaf system when illuminated and the electrolyzer in the dark. The use of a commercial battery and Earth-abundant water-splitting catalysts shows that such a system need not be bespoke, can easily be implemented, and, possibly scaled quickly. Furthermore, the effect demonstrated is not specific to any PV, EC, or battery technology and can be observed as long as the principles of power and voltage matching, as described in the article, are followed. This result holds promise for simple, cost-effective, yet, highly efficient solar water-splitting systems.

As it has been predicted in our earlier work,^[19] the battery can facilitate improvement of STH efficiency in addition to the stabilization function. This gain in STH efficiency is confirmed experimentally with high-efficiency components, appropriate voltage matching, and appropriate power matching of the components. The distribution of the PV current over the diurnal cycle with aid of the battery leads to the increase in STH efficiency from 10.5% to 11.4%. This is a result of reduced electrolyzer current density and related increase in electrolyzer voltage efficiency.

Under periodic irradiance, such as irradiance profiles closer to those found in the field, the artificial leaf system with storage (PEB system) has the potential to outperform an equivalent system without storage in terms of STH efficiency even though adding a battery brings an inevitable potential loss. The lowered electrolyzer current density and persistent electrolyzer operation of a PEB system also have the potential to extend electrolyzer lifetimes and lower the electrolyzer geometric factor when compared with a similar artificial leaf system. Though the gain in efficiency is moderate, it may be relevant when storage is already planned to be part of the system, as an alternative mode of operation. Future work may involve quantifying the gain in the electrolyzer lifetime from this mode of operation and possibly with more economically robust battery technology or simulate the use of grid-linked storage to make such operating modes relevant to mass market hydrogen production.

5. Experimental Section

A seven-cell shingled minimodule for the experiment was prepared using laser-cut silicon heterojunction solar cells. For the full details of the preparation, see the study by Chime et al.^[28] The minimodule with area of 22.4 cm² was coupled with a pair of electrolyzers in series (1.5 cm² NiFeMo symmetric bifunctional electrodes on 1 cm-wide Ni foam strips in 1 M KOH, with onset voltage of 1.5 V each) and, a 160 mAh commercial NMC Li–Po pouch cell battery with a voltage range of 3.7–4.2 V. The pair of electrolyzers was connected in series and treated as a single unit (“the EC”) with an onset voltage of ≈ 3 V.

Preparation of NiFeMo catalyst: The preparation of the trimetal NiFeMo catalyst was based on the procedure of the previous article.^[20] Trimetal NiFeMo catalyst was prepared on an acid-cleaned (3 M HCl) nickel foam (NF) by electrodeposition in a two-electrode electrochemical system. A mixture of precursors consisting of 2.4 M NiSO₄·6H₂O, 0.6 M FeSO₄·6H₂O, 0.2 M Na₂MoO₄·2H₂O, and 0.3 M Na₃C₆H₅O₇·2H₂O was added in 200 mL of ammonia solvent. To prevent unwanted oxidation of metal ions in the precursor solution, N₂ gas was bubbled into the solution for 20 min before conducting electrodeposition. A continuous cathodic current of 160 mA cm^{−2} was applied for 5 min in a two-electrode configuration, where NF and a carbon rod were the working and counter electrode, respectively.

All solvents and reagents were purchased from Sigma Aldrich and used as is. NF was sourced from RECEMAT BV (Ni-5763).

All PV–EC and PEB tests were done under AM1.5 illumination (AM1.5 spectrum, 100 mW cm^{−2}) using a class-A sun simulator from Wacom. This setup allowed for standalone solar cell testing and discharge of the battery across the electrolyzer with voltage and current monitoring individually for each of the solar cell, electrolyzer, and voltmeter. The *I*–*V* curves for the solar cell and electrochemical cells were obtained prior to the test by the four-wire voltage sweep measurements.

Determining the coupling factor of both PV–EC and PEB: The battery was discharged to $\approx 10\%$ state of charge at 3.8 V across the EC. Next, the EC was disconnected and the battery was coupled to the PV module directly. Under illumination the charging voltage of the battery was determined. The approximate coupling factor of the PEB system was then calculated as the battery charging voltage determined the working voltage of the PEB system. Next, the battery was disconnected and the PV was connected to the EC cells directly. Under illumination, the size of the electrolyzer electrodes was adjusted in size to adjust the PV–EC working point voltage to match the calculated coupling factor of the PEB system. The battery was then discharged back to the initial voltage before running the experiment.

The experiment began with the PV–EC measurement (Figure 2. switch A closed and switch B open) for time $t = 30$ s, immediately connecting the battery and beginning the PEB measurement (Figure 2. switch A and B closed) and running it for the same amount of time (t_1), during which charge stored in the battery was counted by the software. At the end of t_1 , switch A was opened and the light source was interrupted, allowing the battery to discharge across the electrolyzer for time t_d . The same method used to count the amount of charge stored was used in reverse to determine the amount of time needed to discharge the battery. The process was repeated an additional two times. Software-based current counting was used to automatically determine the amount of time required to fully discharge the battery to its original state every cycle to fulfill the assumption of 100% battery Coulombic/Faradaic efficiency. The short illumination time was chosen to keep EC degradation to a minimum, as well as keeping state of charge of the battery almost unchanged, so as to keep the system working close to the predetermined coupling factor.

Acknowledgements

The authors would like to thank the silicon heterojunction solar cell baseline; Alain Doumit for the wafer texture and cleaning; Silke Lynen, Volker Lauterbach, and Andreas Mück, for Plasma enhanced chemical vapour deposition; Hildegard Siekmann for Indium Tin Oxide sputtering; and Dr. Andreas Lambertz and Dr. Weiyan Duan for scientific support. The authors would also like to acknowledge the contribution of Christoph Zahren for technical, software support, and guidance. Thomas Birrenbach is also acknowledged for his contribution to the encapsulation of the seven-cell SHJ module. The affiliations have been updated on April 11th 2022.

Open access funding enabled and organized by Projekt DEAL.

Conflict of Interest

The authors declare no conflict of interest.

Data Availability Statement

The data that support the findings of this study are available from the corresponding author upon reasonable request.

Keywords

artificial leaves, batteries, direct coupling, green hydrogen, solar fuels, solar water splitting, solar-to-hydrogen efficiencies

Received: November 2, 2021

Revised: January 11, 2022

Published online: January 27, 2022

- [1] Y. Wang, J. Liu, Y. Wang, Y. Wang, G. Zheng, *Nat. Commun.* **2018**, 9, 5003.
- [2] S. Ardo, D. Fernandez Rivas, M. A. Modestino, V. Schulze Greiving, F. F. Abdi, E. Alarcon Llado, V. Artero, K. Ayers, C. Battaglia, J.-P. Becker, D. Bederak, A. Berger, F. Buda, E. Chinello, B. Dam, V. Di Palma, T. Edvinsson, K. Fujii, H. Gardeniers, H. Geerlings, S. M. H. Hashemi, S. Haussener, F. Houle, J. Huskens, B. D. James, K. Konrad, A. Kudo, P. P. Kunturu, D. Lohse, B. Mei, et al. *Energy Environ. Sci.* **2018**, 11, 2768.
- [3] D. Bae, B. Seger, P. C. K. Vesborg, O. Hansen, I. Chorkendorff, *Chem. Soc. Rev.* **2017**, 46, 1933.
- [4] Z. Wang, C. Li, K. Domen, *Chem. Soc. Rev.* **2019**, 48, 2109.
- [5] Q. Wang, K. Domen, *Chem. Rev.* **2020**, 120, 919.
- [6] C. Jiang, S. J. A. Moniz, A. Wang, T. Zhang, J. Tang, *Chem. Soc. Rev.* **2017**, 46, 4645.
- [7] J. Jia, L. C. Seitz, J. D. Benck, Y. Huo, Y. Chen, J. W. D. Ng, T. Bilir, J. S. Harris, T. F. Jaramillo, *Nat. Commun.* **2016**, 7, 13237.
- [8] Y. Surendranath, D. K. Bediako, D. G. Nocera, *Proc. Natl. Acad. Sci.* **2012**, 109, 15617.
- [9] M. Reuß, J. Reul, T. Grube, M. Langemann, S. Calnan, M. Robinus, R. Schlattmann, U. Rau, D. Stolten, *Sustainable Energy Fuels* **2019**, 3, 801.
- [10] T. Bosserez, J. Rongé, J. van Humbeeck, S. Haussener, J. Martens, *Oil Gas Sci. Technol. Rev. IFP Energies Nouvelles* **2015**, 70, 877.
- [11] J. K. Lee, C. Lee, K. F. Fahy, B. Zhao, J. M. LaManna, E. Baltic, D. L. Jacobson, D. S. Hussey, A. Bazylak, *Cell Rep. Phys. Sci.* **2020**, 1, 100147.
- [12] S. A. Grigoriev, P. Millet, S. V. Korobtsev, V. I. Porembskiy, M. Pepic, C. Etievant, C. Puyenchet, V. N. Fateev, *Int. J. Hydrogen Energy* **2009**, 34, 5986.
- [13] M. Schalenbach, *Int. J. Hydrogen Energy* **2016**, 41, 729.
- [14] S.-H. Hsu, J. Miao, L. Zhang, J. Gao, H. Wang, H. Tao, S.-F. Hung, A. Vasileff, S. Z. Qiao, B. Liu, *Adv. Mater.* **2018**, 30, 1707261.
- [15] C. R. Cox, J. Z. Lee, D. G. Nocera, T. Buonassisi, *Proc. Natl. Acad. Sci. U S A.* **2014**, 111, 14057.
- [16] A. Bergen, L. Pitt, A. Rowe, P. Wild, N. Djilali, *Int. J. Hydrogen Energy* **2009**, 34, 64.
- [17] A. Weiß, A. Siebel, M. Bernt, T. H. Shen, V. Tileli, H. A. Gasteiger, *J. Electrochem. Soc.* **2019**, 166, F487.
- [18] J. D. Maclay, J. Brouwer, G. S. Samuelsen, *Int. J. Hydrogen Energy* **2011**, 36, 12130.
- [19] O. Astakhov, S. N. Agbo, K. Welter, V. Smirnov, U. Rau, T. Merdzhanova, *J. Power Sources* **2021**, 509, 230367.
- [20] M. Lee, B. Turan, J.-P. Becker, K. Welter, B. Klingebiel, E. Neumann, Y. J. Sohn, T. Merdzhanova, T. Kirchartz, F. Finger, U. Rau, S. Haas, *Adv. Sustainable Syst.* **2020**, 4, 2000070.
- [21] B. D. Adams, J. Zheng, X. Ren, W. Xu, J.-G. Zhang, *Adv. Energy Mater.* **2018**, 8, 1702097.
- [22] A. J. Smith, J. C. Burns, J. R. Dahn, *Electrochem. Solid-State Lett.* **2010**, 13, A177.
- [23] A. Angulo, P. van der Linde, H. Gardeniers, M. Modestino, D. Fernández Rivas, *Joule* **2020**, 4, 555.
- [24] A. L. Santos, M.-J. Cebola, D. M. F. Santos, *Energies* **2021**, 14, 3193.
- [25] P. J. McHugh, A. D. Stergiou, M. D. Symes, *Adv. Energy Mater.* **2020**, 10, 2002453.
- [26] C. Lamy, P. Millet, *J. Power Sources* **2020**, 447, 227350.
- [27] J. H. Kim, D. Hansora, P. Sharma, J.-W. Jang, J. S. Lee, *Chem. Soc. Rev.* **2019**, 48, 1908.
- [28] U. Chime, L. Wolf, V. Buga, D. Weigand, A. Gad, J. Köhler, A. Lambert, W. Duan, K. Ding, T. Merdzhanova, U. Rau, O. Astakhov, *Sol. RRL*, 2100594.